

https://doi.org/10.1130/G49745.1

Manuscript received 21 July 2021 Revised manuscript received 3 October 2021 Manuscript accepted 18 November 2021

Published online 3 February 2022

© 2022 Geological Society of America. For permission to copy, contact editing@geosociety.org.

# Non-steady-state slip rates emerge along evolving restraining bends under constant loading

Hanna Elston, Michele Cooke and Alex Hatem\*

Department of Geosciences, University of Massachusetts Amherst, 627 North Pleasant Street, Amherst, Massachusetts 01003, USA

#### **ABSTRACT**

Recent field studies provide evidence of fault slip-rate variability over time periods of 10-100 k.y., yet researchers do not know how processes internal to the fault system (e.g., fault reorganization) impact records of fault slip rates. In this study, we directly observed faultsystem evolution and measured slip-rate histories within a scaled physical experiment of a dextral strike-slip 15° restraining bend representative of a gentle crustal restraining bend. To assess the degree of slip-rate variability at particular sites along the experimental faults, such as would be revealed in a field study, we tracked fault slip rates at specific locations that advected throughout the experiment with accrued fault slip. Slip rates increased or decreased (5%-25% of the applied velocity) both during fault reorganization (e.g., fault growth and abandonment) and as sites migrated to new structural positions. Sites that advected into the restraining bend showed decreased slip rate. While we expect new fault growth to reduce slip rates along nearby fault segments, we document that the growth of new oblique-slip faults can increase strike-slip rates on nearby fault segments. New oblique-slip thrust faults within the experiment accommodated off-fault convergence and unclamped nearby strike-slip segments. The experimental results show that even under a constant loading rate, slip rates at sites located on stable fault segments can vary due to either reorganization elsewhere in the fault system or site advection.

#### INTRODUCTION

Fault slip-rate studies show that slip rates can vary over a wide range of time scales (e.g., Wallace, 1987; Mouslopoulou et al., 2009; Gold and Cowgill, 2011; Zinke et al., 2017, 2019; Gunderson et al., 2018). Previous studies have quantified slip-rate response to some processes, such as glacial (un)loading (e.g., Hetzel and Hampel, 2005) and shifts in regional tectonics (e.g., Federico et al., 2009). However, previous studies have not constrained how slip rates at specific locations or sites along faults respond to processes internal to the fault system, such as fault-strength changes with time (e.g., Dolan et al., 2016) or fault reorganization (e.g., Fattaruso et al., 2016; Matti and Morton, 1993). We investigate and quantify, for the first time, slip-rate response at specific locations or sites

\*Current address: Geologic Hazards Science Center, U.S. Geological Survey, 1711 Illinois Street, Golden, Colorado 80401, USA to nearby fault growth or death (reorganization) and changes in a site's structural position.

Slip-rate response to fault reorganization and a change in a site's structural position are difficult to track in the crust because the geologic record may not preserve clear evidence of these processes and the slip-rate records at sites along nearby faults. In contrast, physical experiments allow us to document fault-system evolution and complete slip-rate histories at every point along faults. Geometric irregularities, such as restraining bends along strike-slip faults, locally reduce slip rates, which facilitates new fault growth and reorganization of the fault system. Numerical and physical experiments of restraining bends have shown that fault-segment growth and abandonment around restraining bends impacts overall strike-slip rates (e.g., Li and Liu, 2007; Cooke et al., 2013; Hatem et al., 2015; Bulkan et al., 2020). However, such studies do not track slip rates at sites along experimental faults as we do here. In this study, we use a scaled physical experiment to directly measure how slip rates at sites along a bend with geometry typical of gentle restraining bends in the crust (e.g., Mann, 2007) respond to fault reorganization and changes in a site's structural position.

# EXPERIMENT SETUP AND FAULT EVOLUTION

We used a tabletop split box apparatus filled with wet kaolin clay to model the evolution of a vertical precut fault (F0) that has a 15° restraining angle and a 2 cm stepover that follows the basal discontinuity (Fig. 1A). The viscosity and strength scaling relationships between the wet kaolin and the crust are such that 1 min in the experiment is equivalent to 1.3-13 k.y. in the crust and 1 cm within the experiment is equivalent to 1-2 km of the crust (Cooke and Van Der Elst, 2012). We followed experimental procedures of Hatem et al. (2015). An overhead camera captured images of the experiment surface at every 0.25 mm of basal plate displacement. We utilized digital image correlation techniques to extract the incremental horizontal displacement and strain field with 1 mm spacing and calculated strike-slip rates along faults. We ran two experiments with identical boundary conditions to assess repeatability. Both experiments produced similar faulting histories and patterns of off-fault deformation (Item S1 in the Supplemental Material<sup>1</sup>).

The faulting history shown in Figure 1B includes multiple periods of fault reorganization. We refer to the initial period of plate displacement needed for strain to localize along fault F0 as the spin-up period and exclude this period from analysis. Following the localization of strain along fault F0, a new dextral strikeslip fault (F1) appears at 24 mm of plate displacement and propagates southward from the western restraining-bend kink. Activity on fault

<sup>1</sup>Supplemental Material. Expanded methodology and repeated experiment faulting history. Please visit https://doi.org/10.1130/GEOL.S.18173555 to access the supplemental material, and contact editing@geosociety.org with any questions. The digital image correlation data of restraining bend experiments are available on the European Plate Observing System (EPOS) repository for analog modeling of geologic processes (Elston and Cooke, 2021).

CITATION: Elston, H., Cooke, M., and Hatem, A., 2022, Non-steady-state slip rates emerge along evolving restraining bends under constant loading: Geology, v. XX, p. , https://doi.org/10.1130/G49745.1

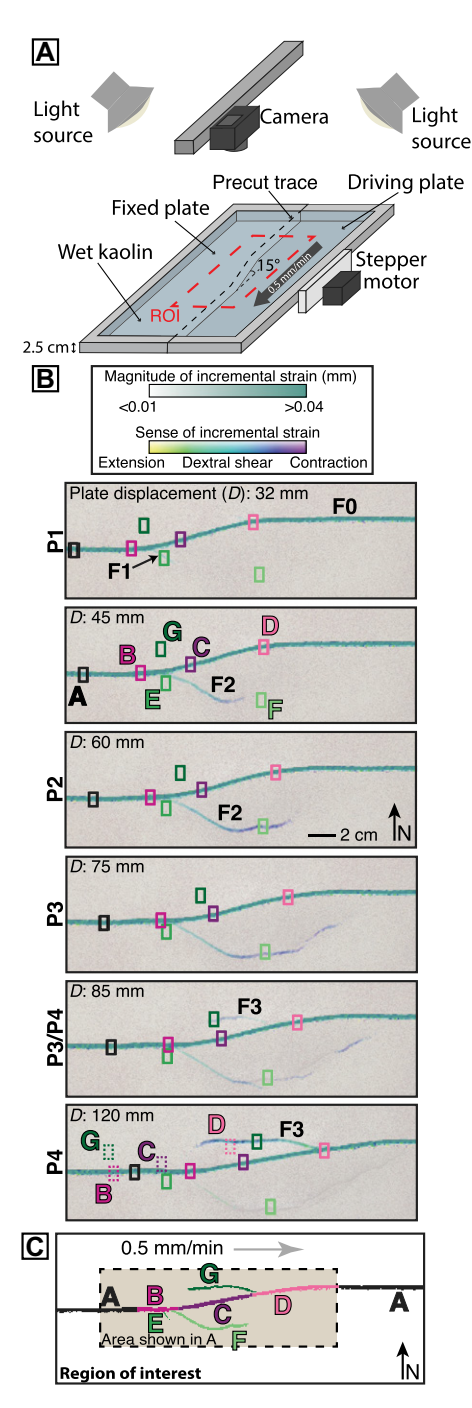


Figure 1. (A) Schematic of the experimental setup. ROI—region of interest. (B) Incremental horizontal strain maps and locations of each site (solid rectangles) throughout the experiment. Hue indicates sense of strain rate, and saturation indicates magnitude. F0 is the precut fault, and F1–F3 are faults that emerged during the experiment; P1–P4 represent periods of fault reorganization (see Figs. 2 and 3). Dashed rectangles show locations of sites B–D and G at 0 mm plate displacement, revealing site advection. North arrow is to simplify the in-text descriptions of changes in fault surface traces. (C) Fault segment map. Colors and letters delineate distinct slip-rate histories.

F1 ceases at 40 mm of plate displacement as a second new dextral fault (F2) appears  $\sim$ 1 cm east of F1 and propagates southeastward. After

45 mm of plate displacement, fault F2 turns and forms new segments striking west and southwest that are subparallel to the restraining segment of fault F0. These distal segments with west and southwest strike accommodate greater contraction than dextral shear. Between 65 and 85 mm of plate displacement, activity on contractional segments of fault F2 decrease while the dextral segment remains active near fault F0. A third new fault (F3) propagates westward from the eastern restraining-bend kink and accommodates both contraction and dextral shear (Fig. 1B, 85 mm plate displacement panel). For the rest of the experiment, fault F3 continues to propagate westward and accommodates increasing strain rates while the dextral strain rates on fault F2 decrease.

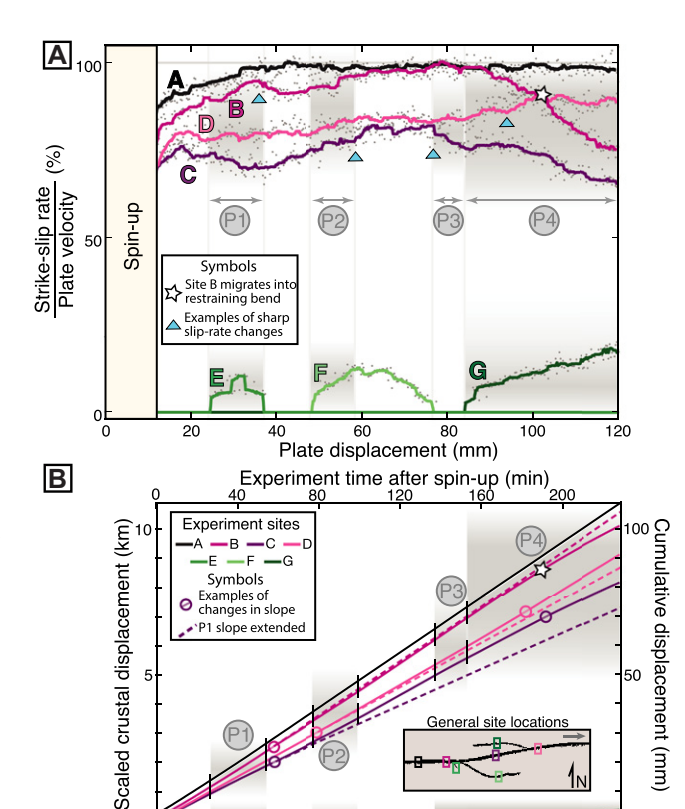
# EXPERIMENTAL SITE SLIP-RATE RESULTS

Not all sites along the restraining bend reveal the same time history of slip-rate variability in the experiment. Using slip-rate histories from all sites, we delineated seven distinct slip-rate histories that map onto different segments of the fault system (Fig. 1C; Item S2). To explore these temporal slip-rate variations, we selected one specific site from each distinct slip history: sites A–D sit along fault F0, and sites E–G capture growth of three new faults. From the site slip-rate histories (Fig. 2A), three first-order observations emerge: (1) cumulative slip recorded at each site varies despite constant loading, (2) sites along

new oblique-slip faults have slower strike-slip rates than all four sites along fault F0, and (3) slip-rate variations at sites along fault F0 correspond to fault-system reorganization.

The early strike-slip rate increase documented at all sites along fault F0 (sites A–D) until 30 mm of plate displacement reflects early fault-zone weakening with accumulating fault slip. For the remainder of the experiment, the slip rate at site A equals the applied velocity due to its distal position from the restraining bend (Fig. 2). In contrast, strike-slip rates at sites B–D fluctuate between 65% and 100% of the plate velocity, and slip rates at sites E–G on faults F1–F3 fluctuate between 0% and 25% of the plate velocity (Fig. 2).

Four episodes of fault reorganization (P1-P4) correspond to slip-rate variations at sites B–D of >5% of the applied velocity (Fig. 2). As fault F1 grows during period P1, the strikeslip rate at site C on the restraining segment decreases. Following the abandonment of fault F1 at site E, site B experiences a sharp decrease in slip rate while the slip rate at site C increases, showing that abandonment of one fault can inhibit or promote slip at nearby sites depending on the site's structural position. Increases in strike-slip rates at sites B-D along fault F0 and site F on fault F2 show a system-wide increase in slip rate with the growth of F2 during period P2. With both the abandonment of fault F2 during period P3 and the growth of F3 (at site G) during P4, the strike-slip rate at site C decreases.



100 150 200 Scaled crustal time (k.y.)

rates (derivatives of lines in B) for sites A-G (see Fig. 1 for site locations). Gray dots report raw strike-slip rates, and colored lines show 11-point medians. Gray boxes bound periods of fault reorganization (P1-P4). (B) Cumulative fault displacement for each site after spin-up (solid lines) and slopes of sites B-D during period P1 extrapolated through experiment (dashed lines). Experimental displacement is scaled to crustal displacement using the strength scaling relationship defined in the text.

Figure 2. (A) Strike-slip

250

50

During period P4, the slip rate at site D increases while the slip rate at site B decreases when site B migrates into the restraining bend (Fig. 2, white star).

The slip rate at site D increases from period P2 through period P4 while slip rates at sites B and C fluctuate above and below their P1 slip rate throughout the experiment (Fig. 2B). Thus, projections of the period P1 slip rates either under- or overestimate the cumulative displacement that sites B–D record at the end of the experiment (Fig. 2B). For site C, the difference in cumulative displacement, which scales to 900 m (9.2 minus 8.3 km) over 285 k.y., represents a 10% difference in long-term strikeslip rate.

# FAULT-REORGANIZATION IMPACT ON SLIP RATE

Changes in slip rate at sites along the precut restraining segment, represented by site C, correlate with changes in off-fault incremental convergence during the experiment associated with the growth and abandonment of faults F2 and F3 (Figs. 2 and 3A). Because changes in both convergence rates at sites and the length of active reverse faults produce changes in the amount of off-fault convergence, we compare the strike-slip rate at site C to the convergence rates at sites F and G as well as the summed incremental convergence along faults F2 and F3

(Fig. 3A). With fault F2 accommodating convergence during period P2, the hanging wall of this new fault experiences incremental dilation, unclamping the precut restraining bend segment and increasing strike-slip rates at site C (Figs. 2 and 3). Conversely, the abandonment of fault F2 leading up to period P3 produces an increase in off-fault incremental convergence, which clamps the precut restraining bend segment and reduces the strike-slip rate at site C. While sites F and G accommodate similar maximum incremental convergence, fault F2 is longer than F3. Consequently, when fault F3 develops during period P4, it accommodates less convergence than F2 during P2, resulting in less change in slip rate along F0 than during P2 (Figs. 2 and 3A).

Locations of high off-fault convergence can indicate subsurface reverse slip (e.g., Hatem et al., 2015). Such patterns suggest that fault F3 links at depth with the western restraining-bend kink and that a fourth new fault is growing at depth outboard of the inactive F2 during period P4 (Fig. 3B). If either fault F3 or the proto-fault fully linked to F0, slip on the precut restraining segment perhaps would significantly decrease between the two link points. Fault connections at depth could explain the decrease in strike-slip rate along the restraining segment (site C) during period P4 (Fig. 2). Thus, the impact of fault reorganization on slip rate depends on the site's

structural position, fault-system configuration, and strain partitioning.

#### IMPLICATIONS FOR CRUSTAL FAULTS

Both the experimental sites and slip records from 10 crustal faults with differing slip sense and locality record some degree of slip-rate variability (Fig. 4). The range of slip-rate variability at the seven sites within the experiment overlap the ranges estimated from crustal studies, suggesting that it is plausible that the processes that drive slip-rate variability within the scaled physical experiment may also drive slip-rate variability within crustal fault systems. While this experiment represents one fault geometry and faults with different geometric irregularities could exhibit different degrees of slip-rate variability, the results demonstrate that fault reorganization at geometric complexities can alter the local strain field and, in turn, fault slip rates. Fault-system reorganization can occur over time and length scales beyond those of this particular scaled experiment. Here, we present fault reorganization as a plausible mechanism for temporal slip-rate variability that can, by similarity scaling (Reber et al., 2020), be extended to a wide range of length and time scales.

Temporal variations in the degree of onversus off-fault convergence can produce slip-rate variations near restraining bends. Within the experiment, increases in on-fault

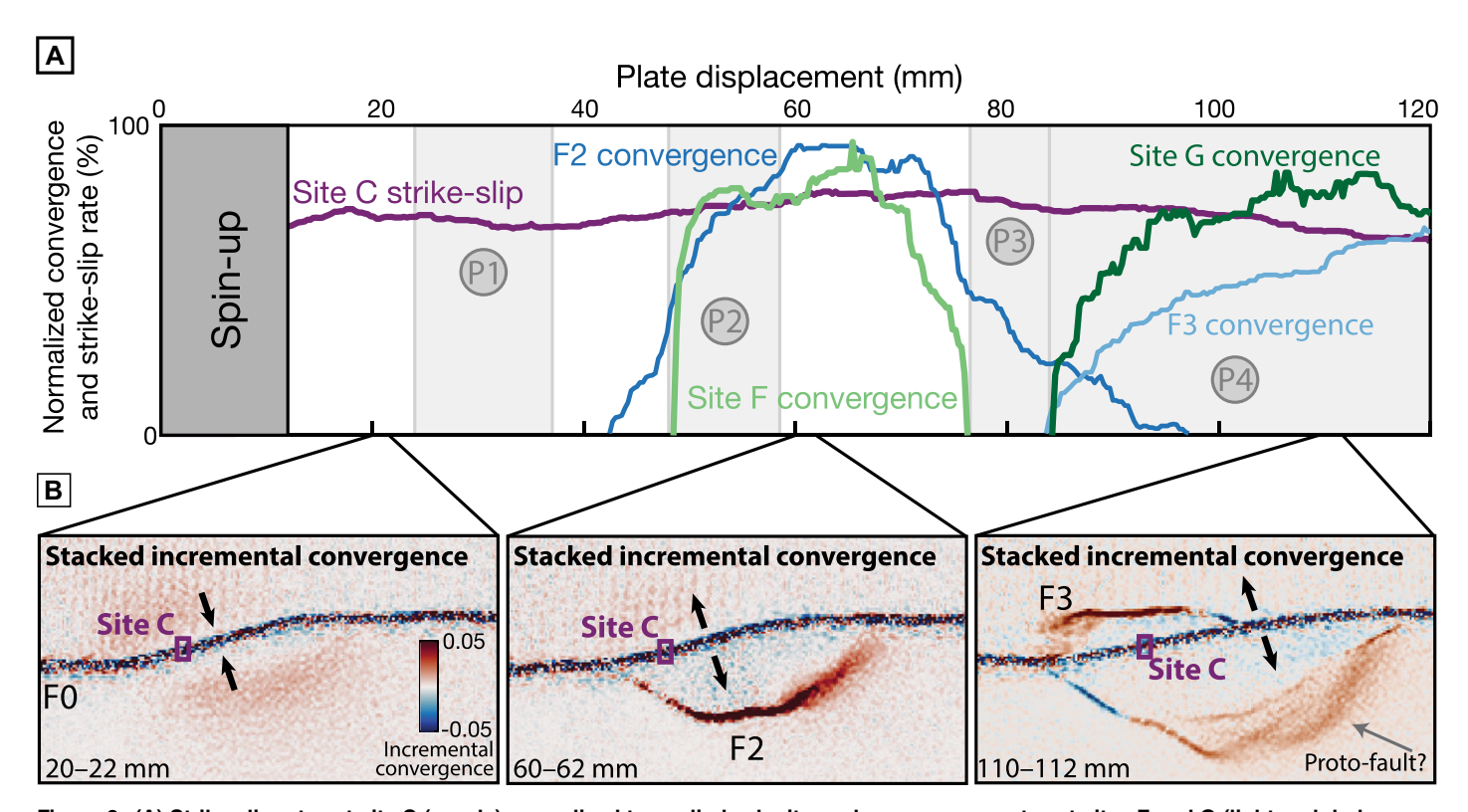


Figure 3. (A) Strike-slip rates at site C (purple) normalized to applied velocity, and convergence rates at sites F and G (light and dark green, respectively) and summed along faults F2 and F3 (dark and light blue, respectively) normalized to maximum convergence rate for sites and faults, respectively. Lines show 11-point medians. (B) Stacked incremental convergence maps show off-fault convergence. Black arrows indicate how off-fault deformation either clamps (inward-pointing arrows) or unclamps (outward-pointing arrows) precut restraining bend. Localized convergence precedes the emergence of upward-propagating faults (Hatem et al., 2015).

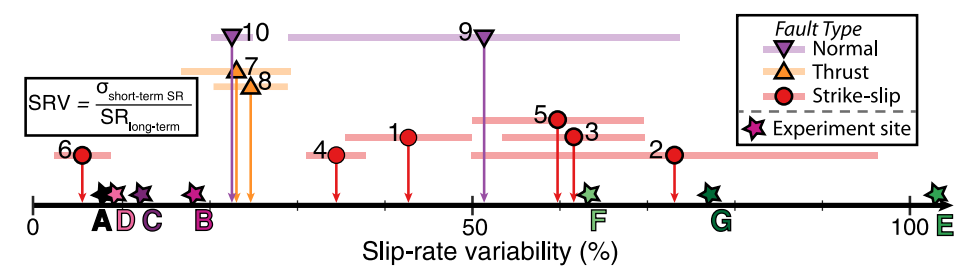


Figure 4. Following the definition of Cowie et al. (2012), slip-rate variability (SRV) depends on standard deviation of short-term slip rates ( $\sigma_{\text{short-term SR}}$ ) for fixed-length windows and long-term slip rate (SR $_{\text{long-term}}$ ). SRV is estimated for 10 previous geologic slip-rate studies (see methods in Item S3 in the Supplemental Material [see footnote 1]). Horizontal bars indicate SRV range from slip-rate uncertainty. Stars report maximum strike SRV from each site of this experimental study. References: 1—Zinke et al. (2019); 2—Dolan et al. (2016); 3—Rittase et al. (2014); 4—Khajavi et al. (2018); 5—Zinke et al. (2017); 6—Chevalier et al. (2012); 7—Yang et al. (2018); 8—Hetzel et al. (2019); 9—McClymont et al. (2009); 10—Schlagenhauf et al. (2010).

convergence during reverse fault growth facilitated slip along unclamped strike-slip fault segments in the hanging wall of the reverse faults. Within the crust, new proto-thrust development, such as has been imaged at the toe of the Nankai trough, offshore Japan (e.g., Moore et al., 1990), may modify patterns in strain partitioning and alter strike-slip rates on faults within the forearc.

Fault slip-rate stability depends on a site's structural position. The experimental results suggest that sites near or within the restraining bend are likely to have greater strike-slip rate variations than sites far from restraining bends (Figs. 2 and 4). Furthermore, sites that have advected to new structural positions within the fault system may record large slip-rate variations. Our experiment maximized site advection by fixing one side of the fault, which replicates conditions at some restraining bends, such as along the Denali fault in Alaska, USA (e.g., Burkett et al., 2016), and the San Andreas fault in California (e.g., Baden et al., 2020). Characterizing the degree of site advection may provide insight into records of temporal slip-rate variability.

A relatively linear fault trace and a lack of nearby faults may promote records of stable slip rates, such as observed at Hokuri Creek (Berryman et al., 2012) along the Alpine fault in New Zealand. In contrast, many of the slip records that show significant variability are from regions with multiple nearby active faults, such as the Marlborough fault system in New Zealand (e.g., Khajavi et al., 2018; Zinke et al., 2019). For such systems, characterizing the history of nearby faults and comparing slip rates measured over similar time intervals (Fig. 2; Item S3) may provide insight on the mechanisms that contribute to slip-rate variability, such as fault reorganization as explored in this study.

### CONCLUSIONS

The scaled physical experiment results of a gentle restraining bend reveal that under constant remote loading, non-steady-state slip rates emerge at sites along restraining bends associated with site advection and fault reorganization. The new approach we present here of tracking slip rates at specific sites facilitates correlation to geologic slip records. While we expect strike-slip rate variations along new fault segments, the experiment results demonstrate that new fault growth can decrease or even increase strike-slip rates on nearby faults that have stable geometry. Along restraining bends, strike-slip rates can increase with new fault growth as the degree of clamping in the hanging wall decreases in response to the new faults accommodating reverse slip. Correspondingly, the abandonment of secondary thrust faults can decrease strike-slip rates along restraining bends. Furthermore, slip rates can vary at specific sites when those sites advect to new structural positions. Consequently, geologic slip-rate studies should consider not only the history of the fault segment investigated but also that of nearby segments as well as site advection history to better understand the processes that drive records of slip-rate variability.

### ACKNOWLEDGMENTS

This research was supported by U.S. National Science Foundation grant EAR 1550133. We thank Austin Elliot, Josie Nevitt, Chelsea Scott, Sarah Titus, and an anonymous reviewer for their constructive reviews.

### REFERENCES CITED

- Baden, C.W., Shuster, D.L., Aron, F., Fosdick, J.C.,
  Burgmann, R., and Hilley, G.E., 2020, Bridging earthquakes and mountain building in the Santa Cruz Mountains, CA: Abstract T056-01 presented at American Geophysical Union Fall Meeting, virtual, 1–17 December.
- Berryman, K., Cooper, A., Norris, R., Villamor, P., Sutherland, R., Wright, T., Schermer, E., Langridge, R., and Biasi, G., 2012, Late Holocene rupture history of the alpine fault in South Westland, New Zealand: Bulletin of the Seismological Society of America, v. 102, p. 620–638, https://doi.org/10.1785/0120110177.
- Bulkan, S., Vannucchi, P., Gasperini, L., Polonia, A., and Cavozzi, C., 2020, Modelling tectonic deformation along the North-Anatolian Fault in the Sea of Marmara: Tectonophysics, v. 794, 228612, https://doi.org/10.1016/j.tecto.2020.228612.
- Burkett, C.A., Bemis, S.P., and Benowitz, J.A., 2016, Along-fault migration of the Mount McKinley restraining bend of the Denali fault defined by late

- Quaternary fault patterns and seismicity, Denali National Park & Preserve, Alaska: Tectonophysics, v. 693, p. 489–506, https://doi.org/10.1016/j.tecto.2016.05.009.
- Chevalier, M.-L., Tapponnier, P., Van der Woerd, J., Ryerson, F.J., Finkel, R.C., and Li, H., 2012, Spatially constant slip rate along the southern segment of the Karakorum fault since 200 ka: Tectonophysics, v. 530–531, p. 152–179, https://doi.org/10.1016/j.tecto.2011.12.014.
- Cooke, M.L., and Van Der Elst, N.J., 2012, Rheologic testing of wet kaolin reveals frictional and bi-viscous behavior typical of crustal materials: Geophysical Research Letters, v. 39, L01308, https://doi.org/10.1029/2011GL050186.
- Cooke, M.L., Schottenfeld, M.T., and Buchanan, S.W., 2013, Evolution of fault efficiency at restraining bends within wet kaolin analog experiments: Journal of Structural Geology, v. 51, p. 180–192, https://doi.org/10.1016/j.jsg.2013.01.010.
- Cowie, P.A., Roberts, G.P., Bull, J.M., and Visini, F., 2012, Relationships between fault geometry, slip rate variability and earthquake recurrence in extensional settings: Geophysical Journal International, v. 189, p. 143–160, https://doi.org/10.1111/j.1365-246X.2012.05378.x.
- Dolan, J.F., McAuliffe, L.J., Rhodes, E.J., McGill, S.F., and Zinke, R., 2016, Extreme multi-millennial slip rate variations on the Garlock fault, California: Strain super-cycles, potentially timevariable fault strength, and implications for system-level earthquake occurrence: Earth and Planetary Science Letters, v. 446, p. 123–136, https:// doi.org/10.1016/j.epsl.2016.04.011.
- Elston, H.M., and Cooke, M., 2021, Digital Image Correlation of evolving restraining bend experiments in wet kaolin: GFZ Data Services, https://doi.org/10.5880/fidgeo.2021.045.
- Fattaruso, L.A., Cooke, M.L., Dorsey, R.J., and Housen, B.A., 2016, Response of deformation patterns to reorganization of the southern San Andreas fault system since ca. 1.5 Ma: Tectonophysics, v. 693, p. 474–488, https://doi.org/10.1016/j.tecto.2016.05.035.
- Federico, L., Spagnolo, C., Crispini, L., and Capponi, G., 2009, Fault-slip analysis in the metaophiolites of the Voltri Massif: Constraints for the tectonic evolution at the Alps/Apennine boundary: Geological Journal, v. 44, p. 225–240, https://doi.org/10.1002/gj.1139.
- Gold, R.D., and Cowgill, E., 2011, Deriving fault-slip histories to test for secular variation in slip, with examples from the Kunlun and Awatere faults: Earth and Planetary Science Letters, v. 301, p. 52–64, https://doi.org/10.1016/j.epsl.2010.10.011.
- Gunderson, K.L., Anastasio, D.J., Pazzaglia, F.J., and Kodama, K.P., 2018, Intrinsically variable blind thrust faulting: Tectonics, v. 37, p. 1454–1471, https://doi.org/10.1029/2017TC004917.
- Hatem, A.E., Cooke, M.L., and Madden, E.H., 2015, Evolving efficiency of restraining bends within wet kaolin analog experiments: Journal of Geophysical Research: Solid Earth, v. 120, p. 1975– 1992, https://doi.org/10.1002/2014JB011735.
- Hetzel, R., and Hampel, A., 2005, Slip rate variations on normal faults during glacial-interglacial changes in surface loads: Nature, v. 435, p. 81–84, https://doi.org/10.1038/nature03562.
- Hetzel, R., Hampel, A., Gebbeken, P., Xu, Q., and Gold, R.D., 2019, A constant slip rate for the western Qilian Shan frontal thrust during the last 200 ka consistent with GPS-derived and geological shortening rates: Earth and Planetary Science Letters, v. 509, p. 100–113, https://doi.org/10.1016/j.epsl.2018.12.032.
- Khajavi, N., Nicol, A., Quigley, M.C., and Langridge, R.M., 2018, Temporal slip-rate stability and

- variations on the Hope Fault, New Zealand, during the late Quaternary: Tectonophysics, v. 738–739, p. 112–123, https://doi.org/10.1016/j.tecto.2018.05.001.
- Li, Q., and Liu, M., 2007, Initiation of the San Jacinto Fault and its interaction with the San Andreas Fault: Insights from geodynamic modeling: Pure and Applied Geophysics, v. 164, p. 1937–1945, https://doi.org/10.1007/s00024-007-0262-z.
- Mann, P., 2007, Global catalogue, classification and tectonic origins of restraining- and releasing bends on active and ancient strike-slip fault systems, *in* Cunningham, W.D., and Mann, P., eds., Tectonics of Strike-Slip Restraining and Releasing Bends: Geological Society [London] Special Publication 290, p. 13–142, https://doi.org/10.1144/SP290.2.
- Matti, J.C., and Morton, D.M., 1993, Paleogeographic evolution of the San Andreas fault in southern California: A reconstruction based on a new cross-fault correlation, *in* Powell, R.E., et al., eds., The San Andreas Fault System: Displacement, Palinspastic Reconstruction, and Geologic Evolution: Geological Society of America Memoir 178, p. 107–159, https://doi.org/10.1130/MEM178-p107.
- McClymont, A.F., Villamor, P., and Green, A.G., 2009, Fault displacement accumulation and slip rate variability within the Taupo Rift (New Zealand) based on trench and 3-D ground-penetrating radar

- data: Tectonics, v. 28, TC4005, https://doi.org/10 .1029/2008TC002334.
- Moore, G.F., Shipley, T.H., Stoffa, P.L., Karig, D.E., Taira, A., Kuramoto, S., Tokuyama, H., and Suyehiro, K., 1990, Structure of the Nankai Trough accretionary zone from multichannel seismic reflection data: Journal of Geophysical Research, v. 95, p. 8753–8765, https://doi.org/10.1029/JB095iB06p08753.
- Mouslopoulou, V., Walsh, J.J., and Nicol, A., 2009, Fault displacement rates on a range of timescales: Earth and Planetary Science Letters, v. 278, p. 186–197, https://doi.org/10.1016/j.epsl.2008 .11.031.
- Reber, J.E., Cooke, M.L., and Dooley, T.P., 2020, What model material to use? A review on rock analogs for structural geology and tectonics: Earth-Science Reviews, v. 202, 103107, https://doi.org/10.1016/j.earscirev.2020.103107.
- Rittase, W.M., Kirby, E., McDonald, E., Walker, J.D., Gosse, J., Spencer, J.Q.G., and Herrs, A.J., 2014, Temporal variations in Holocene slip rate along the central Garlock fault, Pilot Knob Valley, California: Lithosphere, v. 6, p. 48–58, https://doi.org /10.1130/L.286.1.
- Schlagenhauf, A., Gaudemer, Y., Benedetti, L., Manighetti, I., Palumbo, L., Schimmelpfennig, I., Finkel, R., and Pou, K., 2010, Using in situ chlorine-36 cosmonuclide to recover past earth-quake histories on limestone normal fault scarps: A reappraisal of methodology and interpretations: Geophysical Journal International, v. 182,

- p. 36–72, https://doi.org/10.1111/j.1365-246X .2010.04622.x.
- Wallace, R.E., 1987, Grouping and migration of surface faulting and variations in slip rates on faults in the Great Basin province: Bulletin of the Seismological Society of America, v. 77, p. 868–876.
- Yang, H., Yang, X., Huang, X., Li, A., Huang, W., and Zhang, L., 2018, New constraints on slip rates of the Fodongmiao-Hongyazi fault in the Northern Qilian Shan, NE Tibet, from the <sup>10</sup>Be exposure dating of offset terraces: Journal of Asian Earth Sciences, v. 151, p. 131–147, https://doi.org/10.1016/j.jseaes.2017.10.034.
- Zinke, R., Dolan, J.F., Rhodes, E.J., Van Dissen, R., and McGuire, C.P., 2017, Highly variable latest Pleistocene–Holocene incremental slip rates on the Awatere fault at Saxton River, South Island, New Zealand, revealed by lidar mapping and luminescence dating: Geophysical Research Letters, v. 44, p. 11,301–11,310, https://doi.org/10.1002/2017GL075048.
- Zinke, R., Dolan, J.F., Rhodes, E.J., Van Dissen, R., McGuire, C.P., Hatem, A.E., Brown, N.D., and Langridge, R.M., 2019, Multimillennial incremental slip rate variability of the Clarence fault at the Tophouse Road site, Marlborough fault system, New Zealand: Geophysical Research Letters, v. 46, p. 717–725, https://doi.org/10.1029 /2018GL080688.

Printed in USA